

**Hydrogel Nanoparticle Degradation Influences the
Activation and Survival of Primary Macrophages**

Journal:	<i>Journal of Materials Chemistry B</i>
Manuscript ID	TB-ART-04-2021-000982.R1
Article Type:	Paper
Date Submitted by the Author:	15-Jun-2021
Complete List of Authors:	Jarai, Bader; University of Delaware College of Engineering, Chemical and Biomolecular Engineering Stillman, Zachary; University of Delaware College of Engineering, Chemical and Biomolecular Engineering Fromen, Catherine; University of Delaware College of Engineering, Chemical and Biomolecular Engineering

19 **Abstract**

20 The effect of nanoparticle (NP) internalization on cell fate has emerged as an important
21 consideration for nanomedicine design, as macrophages and other phagocytes are primary
22 clearance mechanisms of administered NP formulations. Pro-survival signaling is thought to be
23 concurrent with phagocytosis and recent work has shown increased macrophage survival following
24 lysosomal processing of internalized NPs. These observations have opened the door to
25 explorations of NP physiochemical properties aimed at tuning the NP-driven macrophage survival
26 at the lysosomal synapse. Here, we report that NP-induced macrophage survival and activation is
27 strongly dependent on NP degradation rate using a series of thiol-containing poly(ethylene glycol)
28 diacrylate-based NPs of equivalent size and zeta potential. Rapidly degrading, high thiol-
29 containing NPs allowed for dramatic enhancement of cell longevity that is concurrent with
30 macrophage stimulation after 2-weeks in *ex vivo* culture. While equivalent NP internalization
31 resulted in suppressed caspase activity across the NP series, macrophage activation was correlated
32 with increasing thiol content, leading to increased lysosomal activity and a robust pro-survival
33 phenotype. Our results provide insight on tuning NP physiochemical properties as design handles
34 for maximizing *ex vivo* macrophage longevity, which has implications for improving macrophage-
35 based immune assays, biomanufacturing, and cell therapies.

36

37 **Keywords**

38 Hydrogel nanoparticles, nanoparticle degradation, nanomedicine, macrophages, cell survival,
39 macrophage activation.

40

41 **Introduction**

42 Over the past few decades, interactions of synthetic biomaterials with macrophages, a class of
43 innate phagocytic immune cell, have offered new opportunities to both study cell responses and to
44 modulate cell phenotype with the overall goal of directing host immune response.¹ Certainly,
45 synthetic microenvironments have emerged as powerful tools to study macrophage migration and
46 phenotype progression in the context of disease-altered tissue properties,² with biomaterials-based
47 nano- and microparticle platforms also providing increased understanding of how various
48 internalized physiochemical stimuli drive macrophage function and activation.³⁻⁵ With ever
49 growing advances in synthetic approaches, particulates ranging from lipid-⁶ to metal-⁷ to polymer-
50 based materials^{8, 9} have demonstrated the significance of particle size¹⁰, shape¹¹, modulus¹²,
51 surface charge¹³, and degradability¹⁴ on biological effects of cellular uptake, trafficking, and cargo

52 release. In addition to delivery of known stimuli as therapeutic cargos, particulate platforms afford
53 a unique opportunity to modulate cell phenotype through the cell internalization process, *i.e.*
54 phagocytosis. Innate immune cells, including macrophages, dendritic cells, and neutrophils, are
55 inherently phagocytic, allowing them to engulf foreign materials, and are equipped with high
56 sensitivity at the phagocytic synapse, where everything from surface charge to particle shape can
57 influence subsequent downstream signaling.^{15, 16} Increasing investigation into the role of various
58 physiochemical properties of particulate carriers that alter the phagocytic synapse and downstream
59 signaling is warranted to both improve understanding of the overall process of phagocytosis in
60 these critical innate immune cells and leverage this increased understanding for therapeutic benefit.

61
62 One such physiochemical property deserving of further investigation is particle degradation rate
63 and its effect in the regulation of intracellular signaling following phagocytosis. Our recent work
64 has demonstrated that macrophage lifespan is intimately linked to phagocytic events that can
65 dramatically increase the cell longevity through enhanced lysosomal signaling, even in the absence
66 of cell activation. We previously demonstrated that treatment of inert¹⁷ poly (ethylene glycol)
67 (PEG) diacrylate (PEGDA)-based nanoparticles (NPs) drives pro-survival signaling following NP
68 internalization in a range of *ex vivo* and *in vivo* macrophages.¹⁸ Combined with supporting studies
69 of pro-survival signaling centered in the lysosome,^{19, 20} this prior work highlights an untapped
70 opportunity for intelligently-designed NP platforms to further modulate this response. Upon
71 phagocytosis, the phagosome undergoes compartment acidification and fusion with the lysosome
72 to form the phagolysosome, a strongly acidic and hydrolytic environment enriched with a wide
73 range of enzymes and signaling molecules that are responsible for breakdown of the internalized
74 material and the triggering of subsequent cell activation signaling.^{21, 22} Intracellular NP
75 degradation following phagocytosis has been shown to impact lysosomal signaling and
76 compartment acidification.^{23, 24} Thus, variations in NP intracellular degradation rates may
77 correspond directly to macrophage viability.

78
79 While the particle surface charge and size are known to impact tissue distribution,²⁵ cellular
80 internalization,²⁶ and cellular response,^{27, 28} the role of NP degradability has largely been studied
81 in terms of cargo delivery and sustained release and likely represents an important opportunity
82 for regulation of phagocytotic and subsequent lysosomal signaling. Sustained release of antigens

83 and immune-modifying cargoes have been advantageous in NP vaccination and therapeutic
84 strategies that target phagocytic cells,²⁹⁻³¹ while the renowned stimulatory efficacy of alum, a
85 commonly used vaccine adjuvant, has been attributed in part to its slow degradation profile.³²
86 Despite the many tangential observations that slow-degrading NPs can provide distinct immune
87 stimulation on the cellular level, studies of intracellular degradation of such NP platforms in the
88 absence of therapeutic cargoes are less frequently pursued for sustained phagocyte modulation.
89 Depending on the desired effect (stimulation, suppression, or avoidance), application, or rate of
90 degradation, different NP systems may offer distinct advantages to phagocyte stimulation through
91 controlled degradation,³³ with biodegradable aliphatic polyesters such as polylactic acid (PLA),
92 polyglycolic acid (PGA), poly(lactic-co-glycolic acid) [PLGA], and poly- ϵ -caprolactone (PCL)
93 representing the most widely studied platforms of tunable breakdown. PLGA NPs in particular can
94 have varied rates of degradation based on the ratio of PLA to PGA^{34, 35} and degrade into acidic
95 lactic and glycolic acid-related products that can stimulate the immune system similar to an
96 adjuvant,^{27, 36} with potential for deleterious side effects in some cases.^{37, 38} PCL-based NPs provide
97 slower degradation and gradual cargo release, with no acidic byproducts and thus no autocatalytic
98 degradation,³⁹ providing slow-release profiles with the downside of potential long-term
99 accumulation in the body.⁴⁰ Given the multitude of other NP platforms used for various immune
100 engineering applications, consideration of the degradation rate and associated byproducts of
101 intracellular degradation is likely critical to tuning temporal regulation of phagocytic phenotype
102 and individual lifespan following NP-based cues.

103 Given the role of lysosomal involvement in pro-survival signaling^{19, 20} and the importance of NP
104 design in tuning degradation occurring in the lysosome, we sought to directly investigate the role
105 of tunable particle degradation rates on phagocyte lifespan. In this study, we modulate the
106 degradability of PEGDA-based hydrogel NPs through the inclusion of varying amounts of thiol-
107 PEG-thiol (HS-PEG-SH) in the NP preparation, increasing the acid-sensitivity of the NP and
108 providing more degradable points for the intracellular breakdown. The resulting degradable
109 formulations are investigated to tune the NP-induced survival of primary macrophages. We report
110 that macrophage survival is enhanced following treatment with rapidly degradable NPs relative to
111 their slowly degrading counterparts. This effect is coupled with the upregulation of
112 immunostimulatory molecules likely due to acidic degradation products, as well as increased
113 lysosomal activity and signaling in rapidly degrading NPs. The results provide a platform to tune

114 the *ex vivo* survival of macrophages for a range of applications including biomanufacturing, *in*
 115 *vitro* drug screening assays, vaccine development, and autologous cell therapies.

116

117 **Experimental**

118 *Nanoparticle Synthesis & Characterization*

119 Hydrogel NPs were generated as described previously,⁴¹ but with modifications to pre-particle
 120 compositions. Briefly, to generate 0% HS-PEG-SH, 10% HS-PEG-SH, 20% HS-PEG-SH PEGDA
 121 NPs (referred to as 0%, 10%, and 20% NPs, respectively hereafter), pre-particle mol%
 122 compositions according to **Table 1** were formulated by combining varying amounts of poly
 123 (ethylene glycol) diacrylate (PEGDA) $M_n=700$ (Millipore Sigma), thiol-PEG-thiol (HS-PEG-SH)
 124 $M_n=600$ (Creative PEGWorks), 1,6-hexanediol dimethacrylate (HDDMA) (Millipore Sigma), and
 125 2-carboxyethyl acrylate (CEA) (Millipore Sigma). HDDMA and a higher amount of CEA were
 126 included to improve the resulting hydrogel NP modulus and surface charge, which are notable
 127 differences to our previously used formulations in studying NP-macrophage interactions.¹⁸ 1 mg
 128 of photoinitiator diphenyl(2,4,6-trimethylbenzoyl) phosphine oxide (PI) (Millipore Sigma) and
 129 0.05 mg fluorescent label cyanine 5 (Cy5) maleimide (AAT Bioquest) were added and the
 130 formulations were diluted 1:1 by mass in methanol (Fisher Scientific) to arrive at 50 wt% mixtures.
 131 100 μ l of the mixture was emulsified in 1 mL of silicone oil AP1000 (Millipore Sigma) by vortex
 132 mixing for 1 minute followed by sonicating for 30 seconds. The emulsion was then irradiated with
 133 UV light (APM LED UV Cube, wavelength of 365 nm at a distance of \sim 28 cm from the light
 134 source, \sim 5–10 mW/cm²) for 44, 50, and 52 seconds for 0%, 10%, and 20% NP formulations,
 135 respectively. The polymerized emulsions were washed with 1 ml of n-hexanes followed by two
 136 more washes with 1 ml of ethanol.

137

138 **Table 1:** Final solids compositions of 0%, 10%, and 20% NP formulations, reported in mol%.

NP	Formulation (mol%)	PEGDA	HS-PEG-SH	HDDMA	CEA
0%	0% HS-PEG-SH	75	0	5	20
10%	10% HS-PEG-SH	65	10	5	20
20%	20% HS-PEG-SH	55	20	5	20

139

140

141 *Nanoparticle degradation analysis via Thermogravimetric Analysis (TGA)*

142 In preparation for degradation studies, the synthesized NPs (0%, 10%, and 20%, respectively) were
143 isolated from ethanol via centrifugation at 18,200 RCF for 5 minutes, the ethanol removed, and
144 NPs dispersed into water via vortex mixing for 20 seconds followed by sonication for 30 seconds.
145 This procedure was repeated a second time to ensure removal of ethanol. Following concentration
146 determination via thermogravimetric analysis (TGA) in water using a TA instruments TGA 550,
147 requisite volumes of the three respective NP types (0%, 10%, and 20%) were added to
148 microcentrifuge tubes to achieve concentrations of 3 mg/mL of NPs in 1 ml of the medium of
149 choice (either artificial lysosomal fluid or ALF,⁴² phosphate buffered saline or PBS, ALF with 10
150 mM glutathione or ALF+GSH, or PBS with 10 mM glutathione or PBS+GSH). The NPs were
151 isolated from water via centrifugation 18,200 RCF for 5 minutes. Following isolation, the water
152 supernatant was removed and 1 ml of the medium of choice (either ALF, PBS, ALF+GSH, or
153 PBS+GSH) was added to the microcentrifuge tube. For each NP type (0%, 10%, and 20%), there
154 were 12 total samples (NPs dispersed in each medium with $N = 3$). The NPs were then dispersed
155 via vortex mixing for 20 seconds followed by sonication for 30 seconds and then incubated in a
156 shaker kept at 37 °C and 1000 rpm. At designated time points, a 50 μ l aliquot was analyzed via
157 thermogravimetric analysis (TGA) to determine the mass of non-degraded NPs remaining; select
158 samples were also analyzed via scanning electron microscopy (see sections below).

159

160 *Dynamic light scattering (DLS) and Zeta Potential*

161 DLS of the NPs was performed using a Malvern Zetasizer Nano ZS. NP samples were prepared
162 for DLS measurement by diluting samples in water to ~ 0.1 mg/ml. Hydrodynamic diameters (D_h)
163 and polydispersity indices (PDIs) were measured from two independently synthesized samples.
164 NP samples were prepared for zeta potential measurement by diluting samples in water to ~ 0.5
165 mg/ml in 10 mM NaCl or in PBS. Zeta potentials were measured from two independently
166 synthesized samples.

167

168 *Cryogenic Scanning Electron Microscopy (Cryo-SEM)*

169 As-synthesized 0%, 10%, and 20% NP samples 10 μ L in volume were added to a sample holder
170 for cryo-SEM and flash frozen with liquid nitrogen. Samples were prepared at 3 mg mL⁻¹ for

171 imaging. The samples were sputter-coated for 60 seconds with a platinum coating and then imaged
172 using an Apreo VolumeScope Scanning Electron Microscope at 2 kV from 5,000× to 40,000×
173 magnifications under high vacuum.

174

175 *X-ray Energy Dispersive Spectroscopy (XEDS)*

176 2 µl of PEG-SH NP samples were dropped onto a glass slide and allowed to dry overnight. The
177 samples were then sputter-coated for 65 seconds with gold-palladium coating (thickness of ~5 nm)
178 using a Denton Desk IV Sputter Coater and imaged using a JSM-7400F Scanning Electron
179 Microscope at 3 kV from 1,000× to 40,000× magnifications under high vacuum. XEDS was
180 performed using the JSM-7400F that is equipped with an OXFORD INCAx-sight energy-
181 dispersive XEDS detector. Samples were analyzed for 100 seconds and elemental data collected
182 using the INCA software for elemental analysis.

183

184 *Liquid Chromatography Mass Spectrometry (LC-MS)*

185 Similar to degradation studies, the synthesized NPs (0%, 10%, and 20%, respectively) were
186 isolated from ethanol via centrifugation at 18,200 RCF for 5 minutes, the ethanol removed, and
187 NPs dispersed into water via vortex mixing for 20 seconds followed by sonication for 30 seconds.
188 This procedure was repeated a second time and a third time to ensure removal of ethanol.
189 Following concentration determination via thermogravimetric analysis (TGA) in water using a TA
190 instruments TGA 550, requisite volumes of the three respective NP types (0%, 10%, and 20%)
191 were added to microcentrifuge tubes to achieve concentrations of 3 mg/mL of NPs in 1 ml of water,
192 chosen to prevent ion interference with mass spectrometry. At 1-day, 2-day, 7-day, and 14-day
193 time points, the NPs were isolated from water via centrifugation 18,200 RCF for 5 minutes.
194 Following isolation, the water supernatant was removed for analysis via LC-MS. The particle
195 degradation products were then analyzed using a Q-Exactive Orbitrap coupled with an HPLC.
196 Analysis was then performed in the Xcalibur software and species identified by the authors.

197

198 *Animals*

199 Animals were housed in a pathogen-free facility at the University of Delaware. Studies involving
200 animals were performed according to the National Institutes of Health (NIH) guidelines for the
201 care and use of laboratory animals and were approved by the Institutional Animal Care and Use

202 Committee (IACUC) at the University of Delaware. Female C57BL/6J (Jackson Laboratories) six
203 to twelve weeks of age were used to isolate primary BMMs.

204
205 *Primary cell isolation and culture*

206 Bone marrow-derived macrophages (BMMs) were generated according to standard protocols as
207 previously described.⁴³ Briefly, bone marrow cells from femurs and tibias of mice were plated in
208 BMM differentiation media composed of DMEM/F-12 media (Corning) with 20% fetal bovine
209 serum, 30% L929 cell conditioned media, and 1% Penicillin-Streptomycin. An equal volume of
210 BMM differentiation media was added on day 3 and cells were used on day six for experiments in
211 DMEM/F-12 media containing 10% fetal bovine serum.

212
213 *Assessment of cell viability*

214 BMMs were seeded in 96-well plates (1×10^5 cells/well) and allowed to adhere for at least 4 h prior
215 to NP treatment. BioTek Cytation 5 Multimode Imager was utilized to continuously determine cell
216 counts. Caspase-Glo® 3/7 Assay System (Promega) was used according to manufacturer's
217 guidelines to determine the levels of caspase 3 and caspase 7 in BMMs and luminescence was
218 measured using BioTek Cytation 5 Multimode Imager.

219
220 *NP Internalization and Trafficking*

221 BMMs were plated in 24-well plates (2×10^5 cells/well) and allowed to adhere overnight prior to
222 NP treatment. BMMs were then dosed with 50 $\mu\text{g/ml}$ Cy5-labelled NPs. Cells were detached
223 using Accutase® (Innovative Cell Technologies, Inc.) at 0, 4, 16, 24, 48, and 72 hours (h) and
224 analyzed for %Cy5+ cells using ACEA NovoCyte Flow Cytometer to determine kinetic NP
225 uptake. For lysosomal imaging, BMMs were cultured in glass bottom 96-well plates (1×10^5
226 cells/well) and Cell Navigator™ Lysosome Staining Kit (AAT Bioquest) was used according to
227 manufacturer's guidelines. Cells were imaged using BioTek Cytation 5 Multimode Imager.

228
229 *Macrophage polarization studies*

230 BMMs were plated in 6-well plates (1.5×10^6 cells/well) and allowed to adhere overnight prior to
231 NP treatment. BMMs were then dosed with 100 $\mu\text{g/ml}$ Cy5-labelled NPs. At 24 h and 72 h
232 timepoints, cells were detached using Accutase® (Innovative Cell Technologies, Inc.) and washed
233 twice with PBS supplemented with 2% FBS. Cells were then incubated with anti-CD16/32 (Fc

234 block, Biolegend) for 10 minutes and then stained with CD80-Pacific Blue, CD86-AlexaFluor700,
235 and I-A/I-E-Brilliant Violet 785™ antibodies (All from Biolegend) for 30 minutes in the dark at
236 4°C. Cells were then fixed with 4% paraformaldehyde in PBS (Alfa Aesar) for 15 minutes at room
237 temperature and then permeabilized by washing twice with Intracellular Staining Permeabilization
238 Wash Buffer (Biolegend) and stained with CD206-PE-Cy7 antibodies (Biolegend) and analyzed
239 using ACEA NovoCyte Flow Cytometer.

240

241 *Cytokine analysis*

242 Enzyme-Linked Immunosorbent Assay (ELISA) kits for Interleukin-6 (IL-6), Interleukin-10 (IL-
243 10), and Tumor Necrosis Factor- α (TNF- α) (all from BD Biosciences) were used to determine
244 cytokine concentrations in culture supernatants according to manufacturer's guidelines.

245

246 *Statistical analysis*

247 GraphPad Prism 9 (GraphPad Software Inc) was used to perform all the statistical analyses. All
248 quantitative data are represented as mean \pm standard deviation (SD) or standard error of the mean
249 (SEM). Tukey's multiple-comparisons tests were used to generate p -values in ANOVA multiple
250 comparisons, unless stated otherwise.

251

252

253

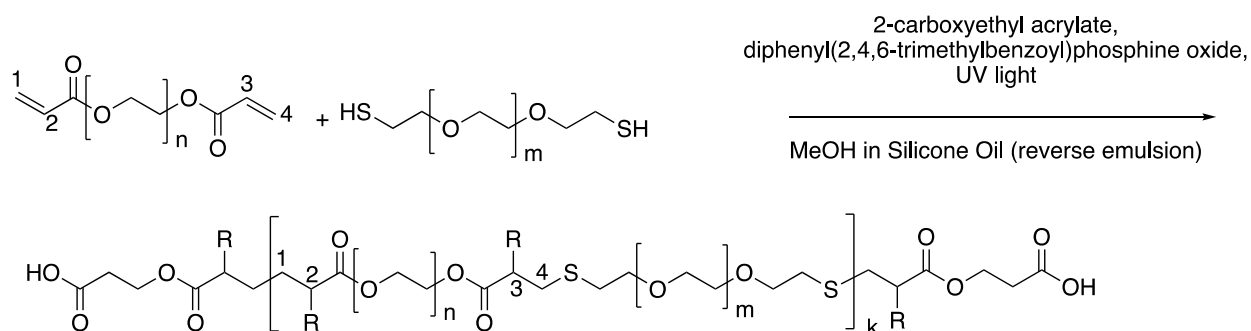
254 **Results & Discussion**

255 *Nanoparticle Synthesis and Characterization*

256 To form a set of NPs that could aid in the determination of the cause and extent of primary cell
257 longevity, we synthesized a set of PEGDA and HS-PEG-SH-based NPs, which had varying
258 amounts of HS-PEG-SH (as described in the Experimental Section). Given the varied thiol content,
259 we hypothesized that these formulations would lead to variable intracellular degradation rates and
260 thus variable longevity of primary cells. The main scheme of NP synthesis is shown in **Figure 1**,
261 which shows the polymerization of PEGDA with HS-PEG-SH being capped primarily by CEA
262 groups at its surface. As shown in **Figure 1**, the polymer NP will primarily be comprised of
263 PEGDA and HS-PEG-SH, with each NP type having a variable amount of HS-PEG-SH (either
264 0%, 10%, or 20% of PEGDA replaced with HS-PEG-SH by mole). The assumption of the reaction

265 scheme is that carbons 1 and 4 react with other with CEA and HS-PEG-SH (PEGDA for the 0%
 266 NPs), respectively, leaving carbons 2 and 3 to react with other molecules such as PEGDA, HS-
 267 PEG-SH (not for the 0% NPs), methanol (hydrogen abstraction), CEA, or Cy5-maleimide (which
 268 are collectively represented as R groups). In reality, there will likely be many varieties of reactions
 269 between the molecules present to form the polymer NPs such that carbons 1-4 can react with many
 270 combinations of the aforementioned molecules, though reactions of PEGDA with itself or with
 271 HS-PEG-SH (for the 10% and 20% NPs), or with the solvent will be much more probable than
 272 reactions with CEA or Cy5-maleimide because of the larger relative number of moles of PEGDA
 273 and HS-PEG-SH since the reaction rates for vinyl carbons in photopolymerization are similar,
 274 though they may have slight effects from steric hindrance in the case of the Cy-5 maleimide.⁴⁴

275
 276

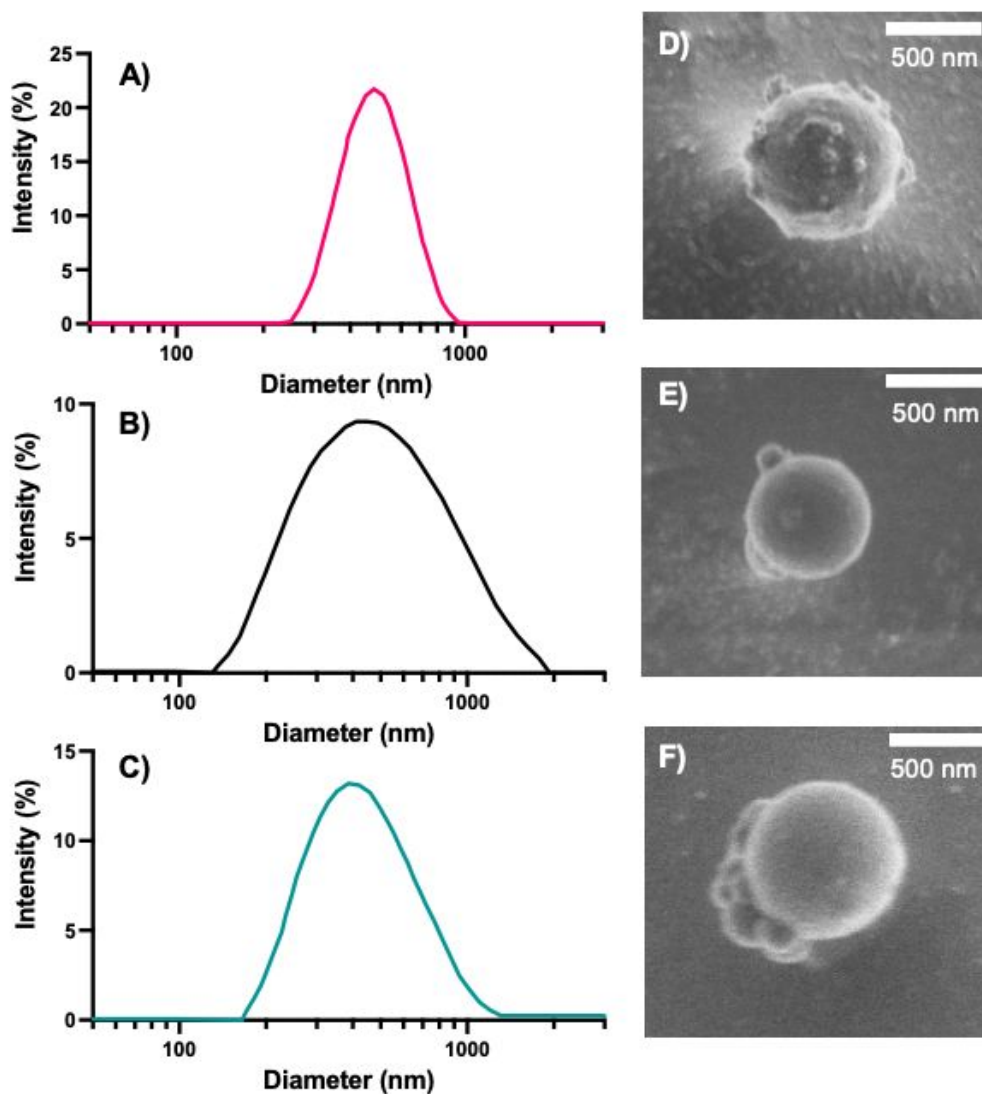


277
 278 **Figure 1:** Representative reaction scheme of PEGDA monomer with HS-PEG-SH to form polymer NPs in
 279 a reverse emulsion where R groups could be PEGDA chains, HS-PEG-SH chains, hydrogen, CEA, or Cy5-
 280 maleimide. Bonds shown can also be via carbons 2 and 3 instead of 1 and 4, as well.

281 Following the synthesis of the 0%, 10%, and 20% NPs, we characterized the NPs via DLS, SEM,
 282 zeta potential, and EDS to obtain NP sizes (DLS, SEM), overall surface charge (zeta potential),
 283 and relative sulfur content (XEDS). Similar to our previous syntheses of PEGDA-based NPs^{18, 41},
 284 the synthesized NPs were typically ~500 nm in diameter, as measured via DLS (**Figure 2A, 2B,**
 285 **and 2C**) and confirmed via SEM (examples shown in **Figure 2D, 2E,** and **2F** and in the SI in
 286 **Figure S1**). The z-average diameters of the three NPs were 524.9 ± 121.6 nm, 467.8 ± 14.3 nm, and
 287 584.3 ± 14.1 nm, respectively, and, as can be seen from the NP size distributions, the sizes and size
 288 ranges for the three NPs are similar, indicating that size will not significantly affect interactions
 289 with cells, nor their internalization. The NP sizes for the three formulations are also within the
 290 desired size range for macrophage phagocytosis ($0.1 - 10 \mu\text{m}$)⁴⁵, which is critical for determination

291 of the effect of variable degradation rates on primary cell longevity and can also affect immune
292 response.^{45, 46}

293



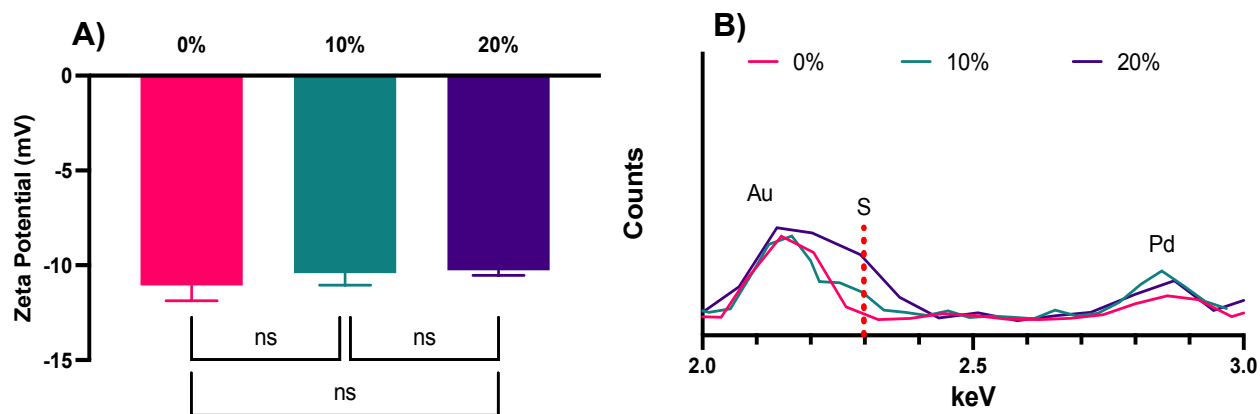
294 **Figure 2:** Intensity distribution of A) 0%, B) 10%, and C) 20% NPs acquired from DLS. Representative
295 cryo-SEM images of D) 0%, E) 10%, and F) 20% NPs.

297
298 The zeta potentials of the NPs, -11.1 ± 0.4 , -10.4 ± 0.6 , and -10.3 ± 0.4 mV, for the 0%, 10%, and
299 20% NPs, respectively (**Figure 3A**), are all negative, as expected of NPs with CEA incorporated
300 into their formulations. The slight differences in zeta potential can likely be attributed to increases
301 in the relative number of thiol groups on the surface of the NPs in the 10% and 20% formulations,
302 which will make them less negative overall, though the values are not statistically significant as
303 determined via Tukey's multiple comparisons as part of a one-way ANOVA. The zeta potentials

304 were also determined in PBS (**Figure S2**), were slightly negative, and not statistically significantly
 305 different, as was the case in NaCl. Regardless of solvent, the zeta potentials are all slightly negative
 306 and not different enough in magnitude to cause significant differences in uptake.²⁶ Other
 307 advantages of their negative surface charge is the reduction of NP aggregation,⁴⁷ increased NP
 308 uptake by phagocytic cells relative to neutral or positively charged NPs,^{13, 48} and lower relative
 309 inflammatory potential relative to positively charged NPs.^{13, 26, 49}

310
 311 To confirm the incorporation of HS-PEG-SH into the 10% and 20% NPs and to confirm the
 312 absence of sulfur in the 0% NPs, XEDS was performed during SEM with results shown for the
 313 0%, 10%, and 20% NPs, respectively, in **Figure 3B** (the full spectra can be found in **Figure**
 314 **S3**). As **Figure 3B** shows, the peak for sulfur for the 20% NPs was the largest relative to the peaks
 315 for other elements present, though still relatively small because of the small amount of sulfur
 316 present in the NPs. The peak height of sulfur for the 10% NPs was between that of the 20% NPs
 317 and the 0% NPs, the latter of which was at baseline, indicating no discernable amount of sulfur
 318 present. This result confirmed that there was variable incorporation of HS-PEG-SH into the 10%
 319 and 20% NPs, as desired.

320



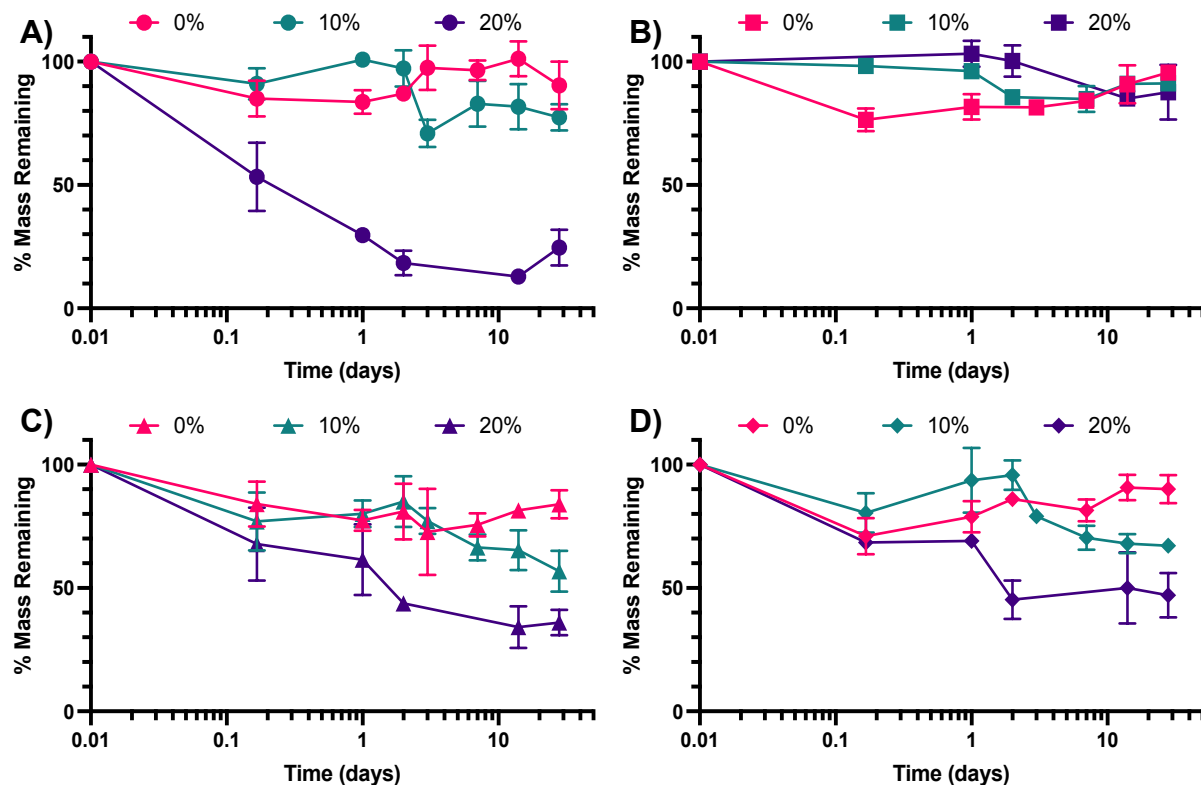
321
 322 **Figure 3:** A) Zeta potential measurements for the 0%-, 10%-, and 20%-SH NPs. The graph shows the mean
 323 and SD from two independently synthesized samples measured 3 times each in 10 mM NaCl solution (6
 324 total measurements, $N=2$). B) Overlapping XEDS spectra of the 0%-, 10%-, and 20%-SH NPs to highlight
 325 differences in the detection of the key sulfur peak between the three NP formulations. Dashed red indicates
 326 main S peak at 2.307 keV.

327

328 *Nanoparticle Degradation*

329 Following the synthesis of the 0%-, 10%-, and 20%-SH NPs, NPs were introduced to variable pH
 330 and glutathione (GSH) amounts to determine their *in vitro* degradation rates. GSH is a reducing
 331 agent that functions to neutralize reactive oxygen species (examples shown in the supporting
 332 information in **Scheme S1A**) and can also function as a nucleophile (examples shown in **Scheme**
 333 **S1B**). The pH buffers were chosen to mimic extracellular pH (~ 7.0 - 7.4)⁵⁰ and intracellular pH in
 334 a phagolysosome (~ 4.5 - 5)⁵¹, which the NPs would encounter upon internalization by a cell such
 335 as a macrophage. The two pH environments are mimicked by PBS (mimicking extracellular, pH
 336 7.4) and artificial lysosomal fluid (ALF, mimicking intracellular, pH 4.5). GSH is commonly
 337 found in the phagolysosome⁵² and thus was added to potentially better mimic the lysosomal
 338 environment in the case of ALF (ALF+GSH medium) or as a point of comparison in the case of
 339 PBS (PBS+GSH medium). The results of the degradation of the three NP types in the four media
 340 (ALF, PBS, ALF+GSH, PBS+GSH) can be found in **Figure 4A** (ALF), **4B** (PBS), **4C**
 341 (ALF+GSH), and **4D** (PBS+GSH) (comparisons between conditions for a single NP type can be
 342 found in the SI in **Figures S4-S6**).

343



344

345 **Figure 4:** Degradation by mass of 0%, 10%, and 20% NPs in A) ALF, B) PBS, C) ALF+GSH, and D)
 346 PBS+GSH. Data points represent the mean and error bars represent the SEM ($N=3$). Comparisons were
 347 made via a two-way ANOVA with Tukey's multiple comparisons.

348
349 As can be seen from **Figure 4B**, none of the NPs experience significant degradation in PBS, which
350 mimics the extracellular environment, up to 28 days. This is consistent with our prior work
351 studying the degradation of similar formulations of PEGDA NPs.⁴¹ The 0% NPs experience some
352 initial degradation from 0 h to 4 h, though this could be the result of partial degradation of NPs
353 prior to dispersion into PBS. Outside of the 4 h time point, the percentage of mass remaining is
354 not statistically significantly different between the three NP types as determined via multiple
355 comparisons as part of a two-way ANOVA. In contrast, for the ALF condition, the 20% NPs are
356 statistically significantly different from the 10% NPs and the 0% NPs at all time points beyond 4
357 h. This would indicate that the 20% NPs are most sensitive to acidic degradation, which, based on
358 the variable chemistries, may indicate that its larger relative percentage of S-C bonds makes it
359 more susceptible to acid-catalyzed degradation. Interestingly, the trends are less clear in the cases
360 of the ALF-GSH and PBS-GSH conditions, for which the 20% NP degradation is not statistically
361 significantly different from the degradation of the 0% or 10% NPs until the 2-day time point.
362 Furthermore, the 10% NP degradation is not statistically significantly different from the
363 degradation of the 0% NPs until the 28-day time point for the PBS-GSH condition or the 14-day
364 time point for the ALF-GSH condition. The extent of degradation for the 20% NPs is less in the
365 ALF-GSH condition and the PBS-GSH condition than in the ALF condition. We hypothesize that
366 this may be the case because, despite the presence of the nucleophilic GSH (particularly in its
367 deprotonated form, GS⁻), the greater concentration of protons in the ALF relative to PBS causes
368 greater protonation of the GSH to keep it in its less nucleophilic, protonated form, which both
369 utilizes the protons in the ALF solution and reduces the ability of the GSH to perform nucleophilic
370 attack to degrade the NPs. In the case of the PBS+GSH, the concentration of protons is
371 significantly lower and thus the proportion of GSH in its deprotonated form will commensurately
372 be much greater than in the ALF+GSH condition. Accordingly, the GSH will more readily be able
373 to perform nucleophilic attack than in the ALF-GSH case. The rates of degradation of the NPs are
374 approximately equal for all three NPs in the ALF-GSH condition and the PBS-GSH condition,
375 which may indicate that the greater activity of the GSH in the PBS-GSH condition counterbalances
376 the relative lack of free protons, which seem to aid in the degradation of the 20% NPs in particular.
377 Overall, our results suggest that variable thiol incorporation does result in variable degradation
378 under relevant intracellular conditions. We expect the degradation rates of the 20% NPs to be the

379 greatest when internalized by cells into low-pH (~4.5-5) phagolysosomes, as our intracellular-
380 mimicking degradation confirms that NP breakdown is highest in all of the conditions studied for
381 the 20% NPs. This is expected since it can not only undergo acid-catalyzed ester hydrolysis but
382 can also undergo nucleophilic attack at the sulfide (-S-C-) bonds, both of which are expected to
383 occur in the phagolysosome.^{53, 54}

384

385 In addition to exploring the degradation rates of the three nanoparticle formulations, we also
386 explored the possible mechanisms and products that could be formed from the degradation of the
387 PEGDA- and HS-PEG-SH-based NPs. From the results of the degradation (**Figures S7 – S20**), we
388 were able to identify many products from the degradation of the 0%, 10%, and 20% NPs (**Table**
389 **S1**), which may influence the longevity of primary cells. Most of the products were PEGDA, HS-
390 PEG-SH, and CEA or combinations therein and were indicative of hydrolysis being the primary
391 breakdown mechanism. Ester hydrolysis was observed from the PEG-based products with losses
392 of 54 MW relative to a base PEGDA or HS-PEG-SH molecule. This corresponds to the mass of
393 the acrylate group ($\text{CH}_2=\text{CH}-\text{C}=\text{O}$, which would also have an -OH group or other nucleophile on
394 the ketone) that has undergone nucleophilic attack and left the remainder of the molecule as the
395 leaving group (which is subsequently protonated). There was also evidence of nucleophilic attack
396 at the more ether-like carbons toward the ends of the HS-PEG-SH as evidenced by mass losses of
397 68 MW. This decrease corresponds to losses of HS- $\text{CH}_2\text{-CH}_2\text{-}$ groups from either end of the HS-
398 PEG-SH followed by protonation of the product PEG. The relative lower abundance of these
399 patterns indicates that hydrolysis is likely the primary mechanism, but the availability of both
400 mechanisms as well as sulfur-based leaving groups allows for more rapid degradation of the 10%
401 and 20% NPs relative to the 0% particles in non-PBS (only) environments. Over the 14-day study,
402 the degradation products of the 10% NPs were very similar to those from the 20% NPs, but
403 generally were generated at a later time point (**Figure S20**). Unsurprisingly, the resultant spectra
404 of 0% NPs, unlike the 10% and 20% NPs, did not contain peaks corresponding to the HS-PEG-
405 SH or its derivatives and thus lacked peaks at m/z of 320, 521, 389, and more.

406

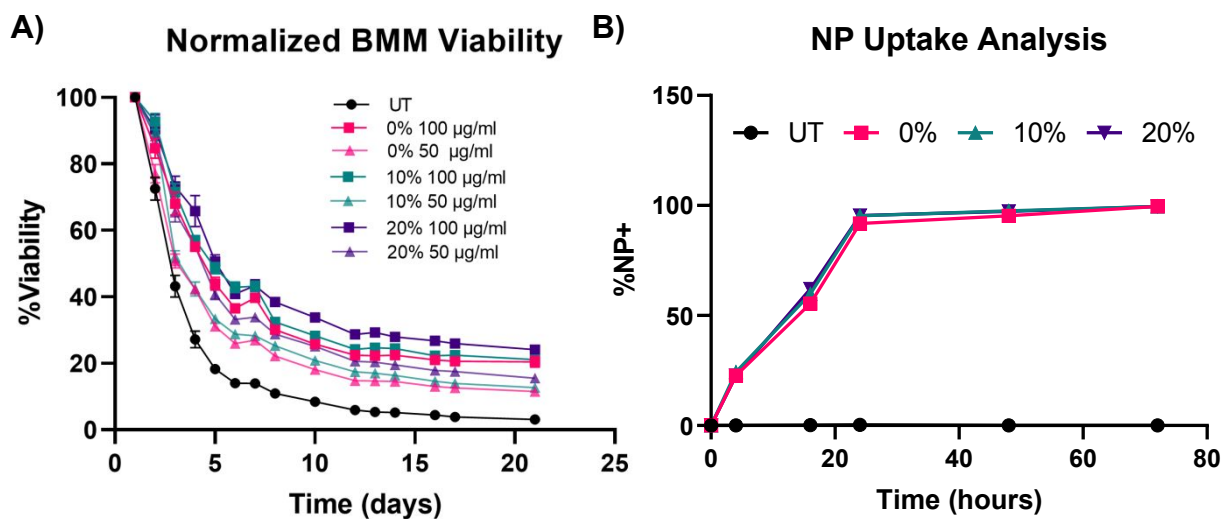
407 *Ex vivo primary macrophage longevity is dependent on NP degradation rate*

408 To test our hypotheses regarding whether NP degradation rate impacts the *ex vivo* survival of
409 primary macrophages, BMMs were dosed with 100 $\mu\text{g/ml}$, 50 $\mu\text{g/ml}$, and 10 $\mu\text{g/ml}$ of the 0%,

410 10%, and 20% NPs and cell counts were continuously monitored following treatment with the
411 different NP formulations (**Figure 5A** and **S5**). In all of the tested formulations, NP treatment
412 enhanced the survival of *ex vivo* BMMs in a concentration-dependent manner. This trend agrees
413 with results from our previous study with other PEGDA-based NPs,¹⁸ even with the notably
414 different additions to the PEGDA NP compositions. Treatment of NPs to BMMs at a concentration
415 of 100 $\mu\text{g/ml}$ resulted in statistically significantly higher %viability than the untreated (UT) cells
416 for the three tested NP formulations as early as 72 h following treatment ($p < 0.05$ using Tukey's
417 multiple comparisons tests as part of a two-way ANOVA). The 0%, 10%, and 20% NP
418 formulations resulted in differences in BMM survival profiles. Overall, rapidly degrading 20%
419 NPs resulted in the highest survival levels over two weeks when compared to the other
420 formulations at the same dosage conditions, which was the case for 100 $\mu\text{g/ml}$, 50 $\mu\text{g/ml}$, and 10
421 $\mu\text{g/ml}$ dosage concentrations. The general pattern of the BMM survival shows greater longevity
422 associated with treatment with 20% NPs followed by treatment with the 10% and 0% NPs,
423 respectively. This suggests that NP degradation rate plays a major role in regulating the survival
424 of the phagocytosing cell. This behavior was evident from treatment with 100 $\mu\text{g/ml}$ and 50 $\mu\text{g/ml}$
425 of NPs, but not for the 10 $\mu\text{g/ml}$ dosage (**Figure S21**), which indicates that there is likely a critical
426 threshold NP dosage required before any effects of internalization and degradation on BMM
427 longevity are observed.

428
429 The results of concentration-dependent cell viability point to the strong effect of the amount of
430 internalized NPs on macrophage survival. Therefore, we investigated whether the enhanced
431 survival following treatment with rapidly degrading 20% NPs relative to its slower degrading
432 counterparts stems from differential uptake across the three NP formulations, as opposed to
433 degradation rate. NP uptake was kinetically quantified via flow cytometric analysis of %Cy5+
434 populations (Representative flow cytometry gating analysis in **Figure S22**). BMM uptake of 0%,
435 10%, and 20% NPs was identical, which was expected since the particles have effectively the same
436 size and charge; after 24 h, more than 90% of the cells were determined to be NP+ following
437 treatment with 0%, 10%, and 20% NPs (**Figure 5B**). More than 95% and 99% of BMMs in all the
438 NP groups were NP+ at 48 h and 72 h after NP dosing, respectively. The rapid and homogenous
439 levels of NP internalization for all of the tested formulations indicates that the differential
440 macrophage survival is unlikely to be occurring due to variations in NP uptake between the three

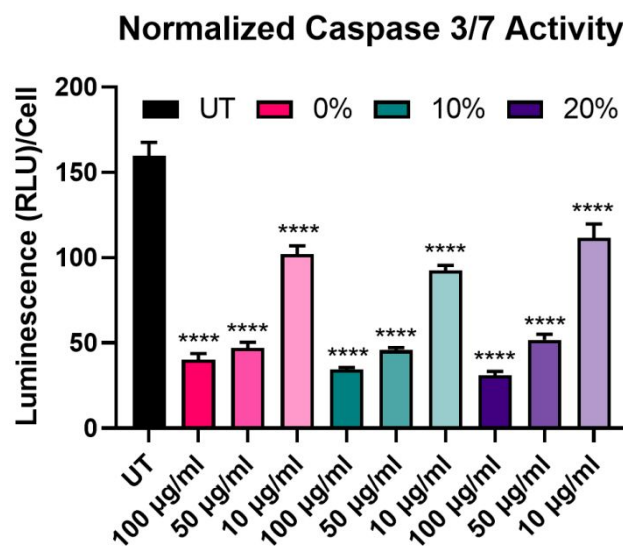
441 NP types. Therefore, other NP-cell interactions are possibly responsible for the enhanced
 442 macrophage survival caused by the internalization of rapidly degrading NPs.



443
 444 **Figure 5:** Effect of NP degradation rate on macrophage survival. A) Normalized cell counts over time of
 445 BMMs treated with 100 µg/ml and 50 µg/ml of 0%, 10%, and 20% NPs ($N=8$) B) Kinetic profiles of BMM
 446 uptake of 0%, 10%, and 20% NP formulations at a concentration of 50 µg/ml ($N=3$). Data points represent
 447 the mean and error bars represent the SEM; error bars are too small to be visible for some data points.

448
 449 After determining that the observed effects of longevity are likely not a result of differences in NP
 450 uptake, we sought to further explore the effects of the degradable NPs on the BMMs. We began
 451 this exploration by investigating the effect of NP degradation rate on pro-apoptotic effectors. We
 452 have previously demonstrated that NP internalization by BMMs enhances survival through the
 453 upregulation of anti-apoptotic Bcl-2 family genes and proteins,¹⁸ which have been shown to
 454 suppress caspase-dependent apoptotic pathways.⁵⁵ Caspase-3/7 activity was measured in BMMs
 455 treated with 100 µg/ml, 50 µg/ml, and 10 µg/ml of 0%, 10%, and 20% NPs and caspase-3/7 activity
 456 was normalized to the corresponding cell count in each group (**Figure 6**). Unsurprisingly,
 457 untreated BMMs exhibited the highest levels of active caspases-3/7, which indicates the strong
 458 apoptotic potential of *ex vivo* macrophages.⁵⁶ Active caspase-3/7 levels were statistically
 459 significantly reduced following dosage with 0%, 10%, and 20% NP formulations at all of the tested
 460 concentrations ($p<0.0001$ for all the NP groups compared to untreated BMMs using Tukey's
 461 multiple comparisons tests as part of a two-way ANOVA). Suppression of pro-apoptotic caspase-
 462 3/7 expression following NP treatment occurred in a concentration-dependent manner, where
 463 treatment with 100 µg/ml of 0%, 10%, and 20% NPs resulted in the greatest reduction of active

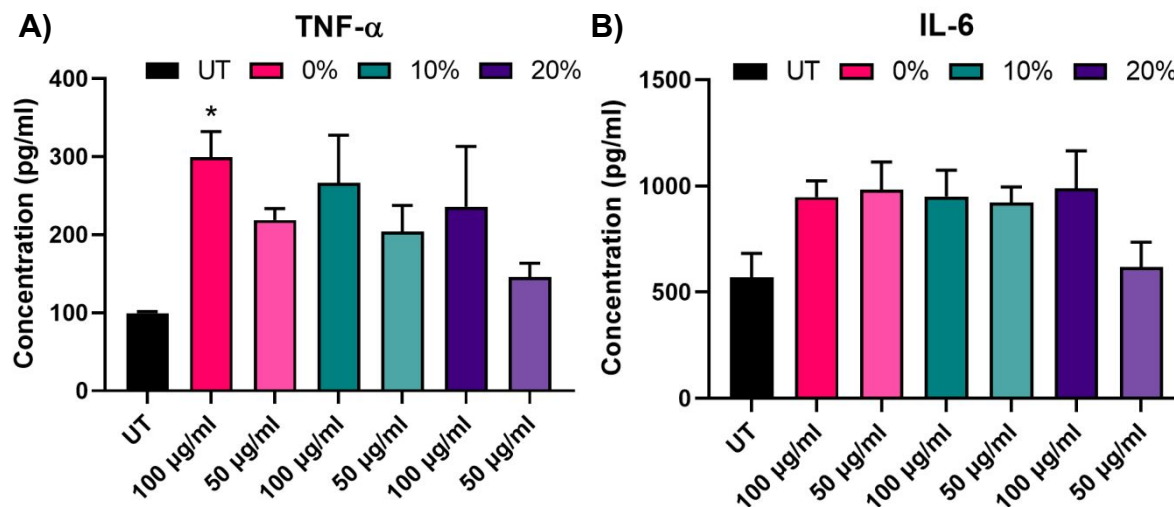
464 caspase-3/7 levels while the treatments at 10 $\mu\text{g/ml}$ concentrations resulted in the least.
 465 Surprisingly, active caspase-3/7 levels did not statistically significantly differ among the 0%, 10%,
 466 and 20% NP formulations at this 72 hr timepoint when dosed at the same concentration ($p>0.05$
 467 using Tukey's multiple comparisons tests as part of a two-way ANOVA). This result contrasts
 468 with the cell viability data (**Figure 5A**), which showed significant differences in %viability
 469 between the 0%, 10%, and 20% NP groups, where the NPs with the highest rates of degradation
 470 resulted in the greatest cell survival. The disagreement between cell viability data and suppression
 471 of pro-apoptotic signaling for the 0%, 10%, and 20% NP groups indicates the possible involvement
 472 of alternate pathways that promote cell survival independent of those relying on caspase-3/7
 473 suppression, which may possibly include cell activation markers.



474
 475 **Figure 6:** Cell count-normalized caspase-3/7 activity in BMMs treated with 100 $\mu\text{g/ml}$, 50 $\mu\text{g/ml}$, and 10
 476 $\mu\text{g/ml}$ of 0%, 10%, and 20% NPs 72 h following NP treatment. **** $p<0.0001$ comparison to UT using
 477 Tukey's multiple comparisons tests as part of a one-way ANOVA ($N=3$). Error bars represent SEM.

478
 479 We next assayed BMMs 2 weeks following NP treatment with 0%, 10%, and 20% NPs to
 480 investigate the effect of NP dosing on macrophage stimuli responsiveness. The effects of 24 h
 481 pulsing with 25 ng/ml LPS of untreated and NP-treated BMMs on IL-6 and TNF- α inflammatory
 482 cytokine secretion was monitored via ELISA (**Figure 7A, B**). Treatment with 0%, 10%, and 20%
 483 NPs, especially at the 100 $\mu\text{g/ml}$ concentration, resulted in notably higher IL-6 and TNF- α , though
 484 only TNF- α secretions for 0% NPs were statistically significantly higher than those of untreated
 485 BMMs. Nonetheless, all of the tested conditions showed responsiveness to LPS stimulation as
 486 evident by the detectable levels of inflammatory cytokines compared to undetectable secretions in

487 the unstimulated counterparts. This indicated that surviving BMMs at two weeks were still stimuli
 488 responsive and presented with functional phenotypes that were enhanced over the UT controls.
 489



490 **Figure 7:** TNF- α and IL-6 concentrations of BMM supernatants two weeks following treatment with 0%,
 491 10%, and 20% NP formulations after a 24 h LPS challenge. * $p < 0.05$ comparison to UT using Tukey's
 492 multiple comparisons tests as part of a one-way ANOVA ($N=3$). Error bars represent SEM.
 493

494 *NP degradation rate promotes the activation of BMMs into an M1-like state*

495 We next probed the effect of degradable NPs on cellular response by investigating whether NP
 496 degradation rate plays a role in the activation of macrophages. BMMs were dosed with 100 μ g/ml
 497 of the 0%, 10%, and 20% NP formulations and flow cytometric analysis of macrophage activation
 498 markers of the M1 and M2 paradigm was executed on BMMs 24 h and 72 h following treatment.
 499 Median fluorescence intensity (MFI) as a measure of activation marker expression was recorded
 500 (Representative flow cytometry gating analysis in **Figure S22**). Relative to untreated BMMs, all
 501 three NP formulations sharply increased the expression of CD86 costimulatory molecule
 502 ($p < 0.0001$ using Tukey's multiple comparisons tests as part of a one-way ANOVA) at both the 24
 503 h and the 72 h timepoints (**Figure 8A, B**), indicating potent activation of BMMs following
 504 treatment with 0%, 10%, and 20% NP formulations. The slowly degrading 0% NPs resulted in the
 505 smallest increase in CD86 expression, while the 10% and 20% NPs with faster degradation resulted
 506 in higher expression at the 24 h and 72 h timepoints. The NP-induced upregulation of CD86 is
 507 accompanied by a statistically significant increase in the expression major histocompatibility
 508 complex class II (MHCII) as early as 24 h, which is even further augmented at 72 h following NP
 509 treatment (**Figure 8C, D**). Similar to CD86 expression, the upregulation of MHCII was observed

510 to be dependent on NP degradation rate, where 10% and 20% NPs were superior to 0% NPs.
511 Overall, the 72 h results showed dramatic increases in the two M1 activation markers, indicating
512 the strong kinetic effects of degradable NPs on macrophage activation, which correspond to
513 notable breakdown from *in vitro* degradation studies. It is noteworthy to mention that significant
514 stimulatory effects with 0% NPs contrast with our previous studies of macrophage phenotypical
515 changes in response to internalization of NPs formulated with PEGDA- and CEA-only. This is
516 likely due to changes in NP formulations, namely the inclusion of HDDMA co-monomer and
517 increase in the amount of CEA used, which are hypothesized to account for the differences between
518 the two formulations. Interestingly, CD80 expression was mostly unchanged 24 h following NP
519 treatment and was suppressed at 72 h (**Figure S23**). This could be in part due to the naturally lower
520 abundance and the sluggish response of CD80 relative to CD86.⁵⁷ CD86, along with other
521 activation markers, has been shown to be stimulated in dendritic cells upon interactions with
522 polymeric particles of varying extents of degradation;⁵⁸ however, it is unclear whether the
523 degraded particles affect the survival of the primary dendritic cells.

524
525 In addition to the upregulation of M1 activation markers in BMMs following the treatment with
526 the three NP formulations, an M2 marker, CD206, was significantly downregulated at both 24 and
527 72 h following treatment with 0%, 10%, and 20% NPs (**Figure 9A, B**), indicating a potent
528 activation towards an M1 phenotypical state. Similar to patterns observed with CD86 and MHCII
529 markers, NP degradation rate played a crucial role in the downregulation of CD206. At the 24 h
530 analysis timepoint, rapidly degrading 20% NPs resulted in the greatest suppression of CD206
531 expression relative to untreated BMMs ($p < 0.0001$ using Tukey's multiple comparisons tests as
532 part of a one-way ANOVA). The suppression of CD206 expression by 10% NPs was the second
533 highest followed by that of the 0% NPs ($p < 0.001$ and $p < 0.01$, respectively using Tukey's multiple
534 comparisons tests as part of a one-way ANOVA). These results were less pronounced at the 72 h
535 timepoint, with the 20% NPs holding the pattern of the sharpest decrease in CD206 expression
536 relative to untreated BMMs ($p < 0.01$), while 0% and 10% NPs were statistically insignificant
537 relative to untreated BMMs ($p > 0.05$), indicating that rapidly degrading NPs play a major role in
538 controlling the macrophage phenotype. This also potentially explains the enhanced primary
539 macrophage survival following internalization of rapidly degrading NPs.

540

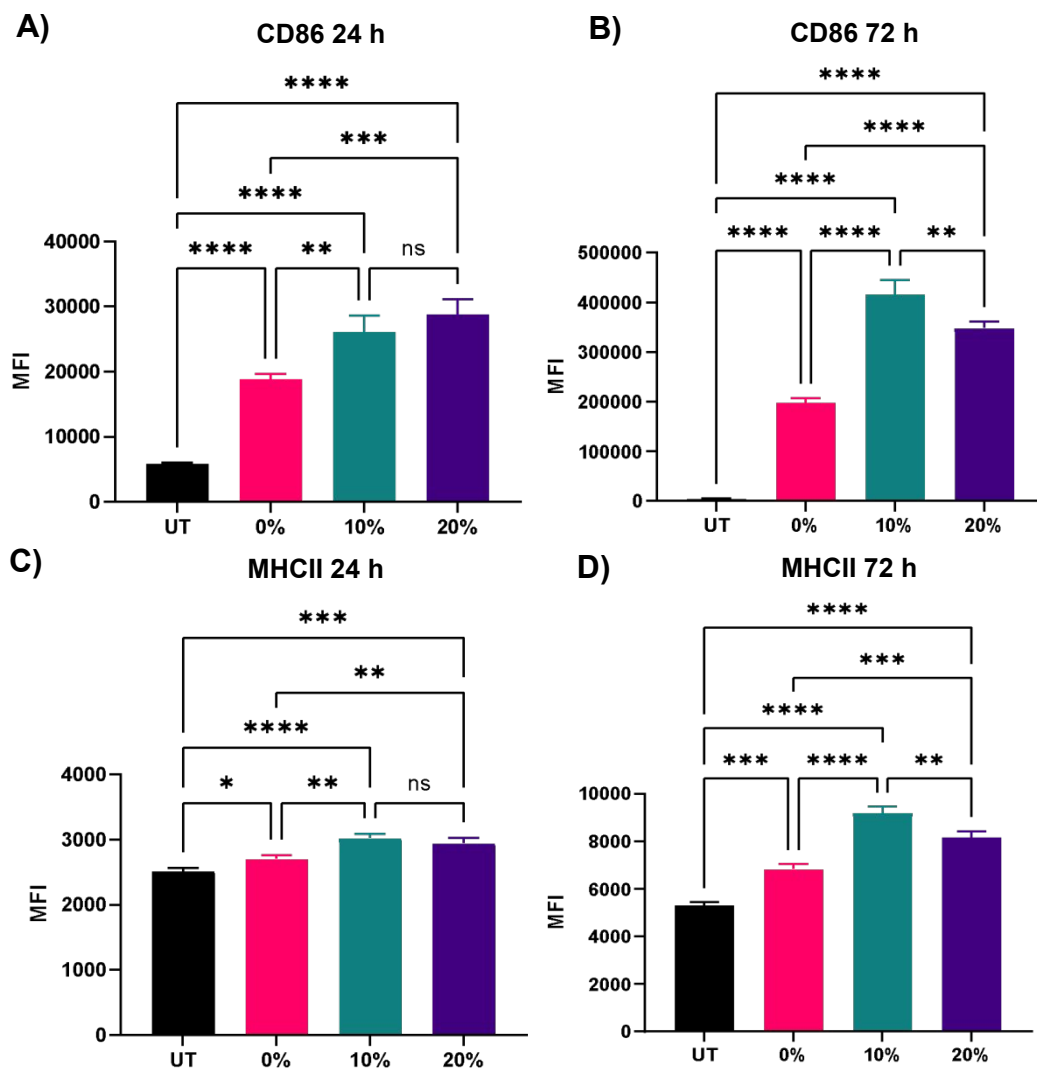
541 Interestingly, IL-6 and TNF- α inflammatory cytokines were not present in supernatants of
542 untreated and NP-treated BMMs within 72 h of NP dosing, with cytokine concentrations below
543 the detectable limit via ELISA analysis (data not shown). While the absence of secretions may be
544 surprising given the potent stimulation of CD86 and MHCII markers, the lack of potent toll-like
545 receptor (TLR) agonists and pathogen-associated molecular patterns (PAMPs) in the NP
546 formulations, which are often required for a robust secretory response,⁵⁹ may explain the
547 undetectable cytokine levels. In addition, while detectable, IL-10 levels in supernatants of
548 untreated and NP-treated BMMs were statistically indistinguishable 72 h following NP treatment
549 (**Figure S24**) ($p>0.05$ using Tukey's multiple comparisons tests as part of a one-way ANOVA),
550 indicating the inability of 0%, 10%, and 20% NPs to stimulate either pro- or anti-inflammatory
551 cytokine secretions. These results are in agreement with low inflammatory cytokine secretion
552 profiles of macrophages upon interactions with PEG-based materials.¹⁷

553

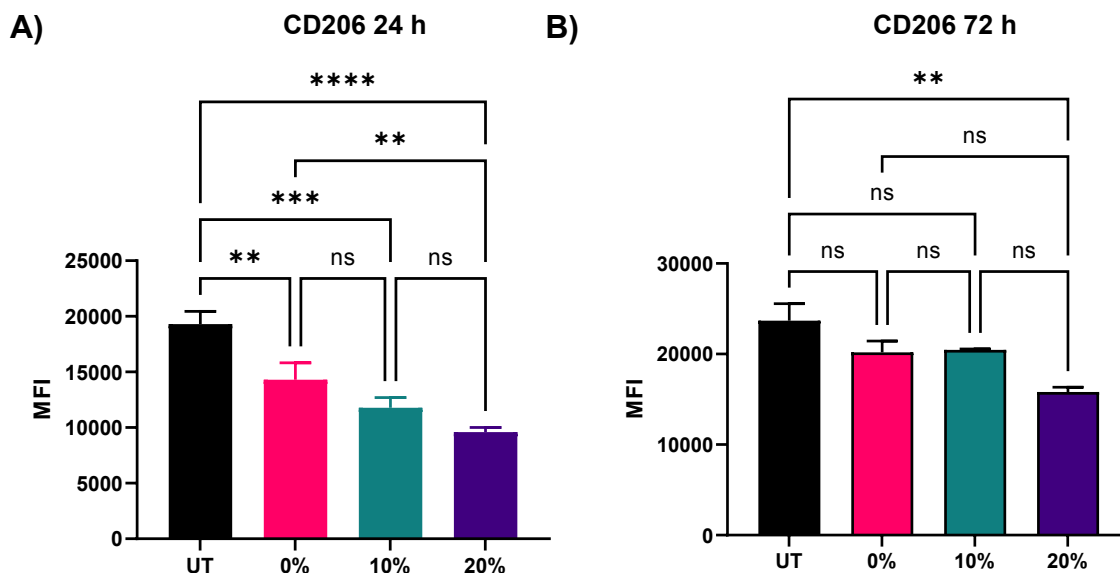
554 The results of immunostimulatory behavior stemming from NP degradation rate present a contrast
555 to other PLGA-based degradable particles, which caused the downregulation of M1 markers
556 including both CD86 and MHCII and was attributed to immunomodulatory acidic degradation
557 products, namely lactic acid.⁶⁰ On the other hand, degradable poly(beta-amino-ester) (PBAE)
558 particles provide supporting evidence of M1-like stimulation in dendritic cells, but does not point
559 to any survival effects as a result of the degradable particle-induced stimulation.⁵⁸ These reports
560 of enhanced immune stimulation may also be because of intracellular processing of specific
561 degradation products of the particles. Therefore, the degradation products of the 0%, 10%, and
562 20% NPs could play an instrumental intracellular role in causing the activation of macrophages as
563 seen by the potent upregulation of CD86 and MHCII M1 markers and the downregulation of
564 CD206 M2 marker. Further investigations are required to understand the direct impact, if any, of
565 NP degradation products on inherent adjuvanticity of these platforms in driving the activation state
566 of macrophages and its link to cell survival. The direct effect of NP degradation on cell survival is
567 contrary to our initial hypothesis that slowly degrading NPs will enable sustained effects relative
568 to rapidly degrading NPs, especially when compared to slowly degrading NPs for antigen delivery
569 and cargo release applications³⁰; this likely is attributed to the stimulation of the intracellular
570 degradation products driving an M1 phenotype.

571

572



573 **Figure 8:** Expression of representative M1 activation markers of BMMs treated with 100 µg/ml of 0%,
 574 10%, and 20% NPs **A)** 24 h CD86 expression **B)** 72 h CD86 expression **D)** 24 h MHCII expression **E)** 72
 575 h MHCII expression. * $p < 0.05$, ** $p < 0.01$, *** $p < 0.001$, **** $p < 0.0001$, ns=not significant using Tukey's
 576 multiple comparisons tests as part of a one-way ANOVA ($N=3$). Error bars represent SEM.



577 **Figure 9:** Expression of CD206 M2 activation marker of BMMs treated with 100 µg/ml of 0%, 10%, and
 578 20% NPs **A)** 24 h **B)** 72 h following treatment. ** $p < 0.01$, *** $p < 0.001$, **** $p < 0.0001$, ns=not significant
 579 using Tukey's multiple comparisons tests as part of a one-way ANOVA ($N=3$). Error bars represent SEM.

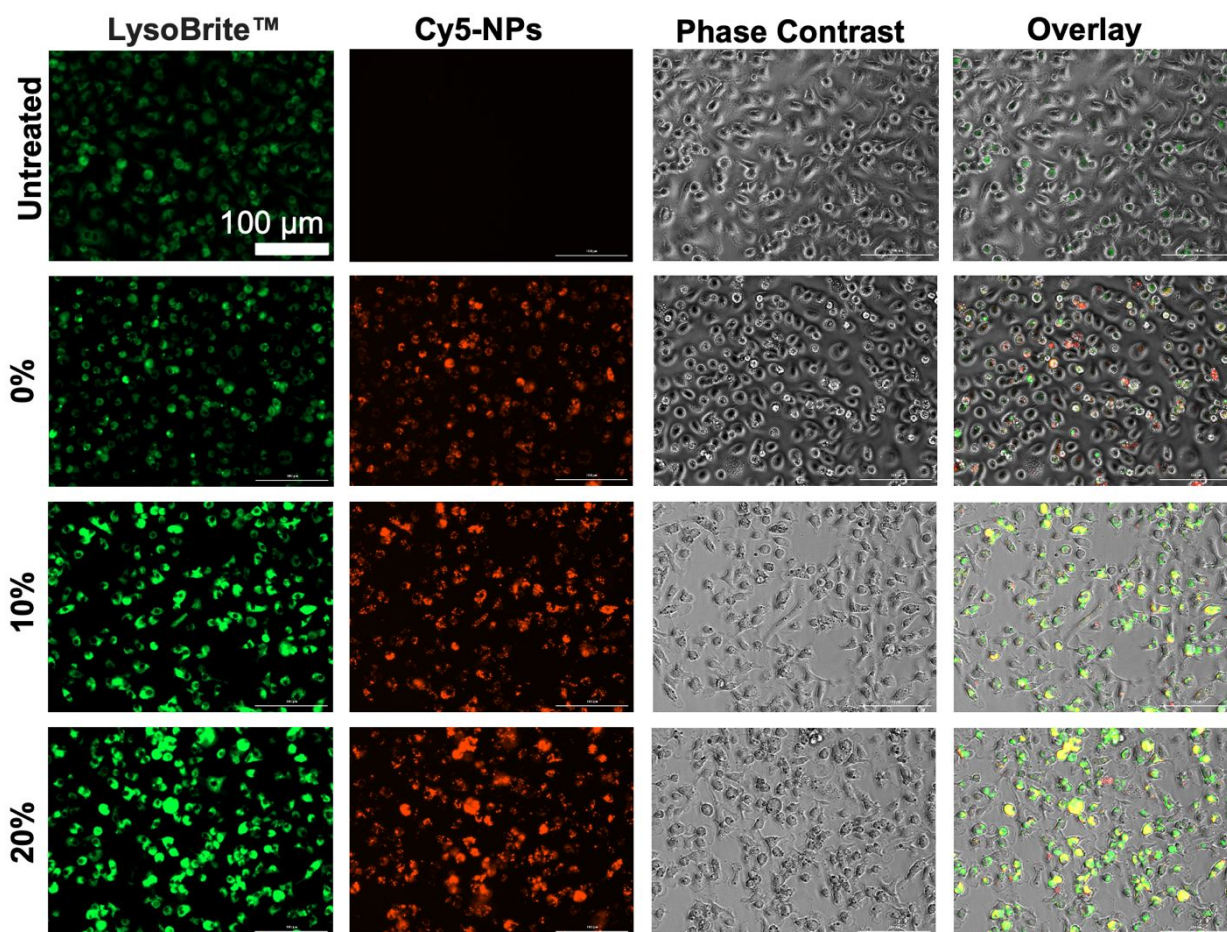
580
 581

582 *Lysosomal activity is enhanced with degradable NPs*

583 Lysosomal tracking was utilized to gain insight on the intracellular trafficking of degradable NPs
 584 and to determine whether NP degradation rate affects intracellular NP processing. Imaging
 585 analysis revealed high intensity LysoBrite™ Green activity in all NP-treated BMMs as compared
 586 to their untreated counterparts, which is indicative of NP trafficking in late lysosomal
 587 compartments (**Figure 10**), especially given the strong overlap between LysoBrite™ Green and
 588 NP fluorescence signals. From LysoBrite™ Green fluorescence, lysosomal activity was strongest
 589 in BMMs treated with 20% NPs followed by activity in the 10%, 0%, and untreated conditions,
 590 respectively, as evident by the bright green fluorescence. As a result, imaging showed drastically
 591 increased lysosomal activity in BMMs dosed with rapidly degradable NPs as compared to those
 592 dosed with slowly degrading NPs or untreated conditions. This observation is expected, as
 593 degradation of phagocytosed materials occurs following the fusion of the phagosome with the
 594 lysosome.⁶¹ We have previously shown that NP internalization stimulates the expression of late
 595 endosomal/lysosomal adaptor, MAPK and mTOR activator (LAMTOR) genes and proteins,¹⁸
 596 which have been linked to survival.^{62, 63} The enhanced lysosomal activity may potentially trigger
 597 increased expression of lysosomal signaling proteins, which have been reported to contribute to

598 cell survival. Administration of biodegradable NPs with acidic byproducts have been shown to
599 restore lysosomal acidity and degradative capacity,^{23, 24} which may further contribute to cell
600 stimulation. Potent activation of lysosomal signaling by degradable NPs may explain the resulting
601 enhanced survival and could provide insight to possible links to macrophage activation evident by
602 the upregulation of CD86 and MHCII and the subsequent enhancement of antigen presentation
603 and interface with adaptive immune cells, which has been shown in dendritic cells⁶⁴ and could
604 extend to macrophage behavior upon phagocytosis and processing of NPs.

605



606 **Figure 10:** Lysosomal tracking with LysoBrite™ Green and imaging at 20x magnification of BMMs treated
607 with 100 μg/ml of 0%, 10%, and 20% NPs 72 h NP treatment. Images are representative of two experiments.
608

609 Overall, based on mass-based degradation profiles of 0%, 10%, and 20% NPs, the 20%
610 formulation experienced the greatest levels of degradation in acidic and reducing environments
611 that simulate lysosomal fluids, with drastic mass loss occurring as early as 24 h following
612 incubation. These results correspond to improved cell survival and enhanced expression of

613 activation markers, likely as a result of increased lysosomal stimulation. The initial enhancement
614 from rapidly degrading 20% NPs result in cell survival beyond 2 weeks, whereas the 0% and 10%
615 NPs of slower rates of degradation are associated with lower lysosomal involvement and
616 enhancement of activation signaling. Therefore, while pro-survival cues may be present from all
617 treatment conditions, including those of slowly degrading NPs, they may not be sufficient to
618 overcome the initial boost from the rapidly degrading 20% NPs. Extended phagocyte viability
619 following phagocytosis has often been observed following internalization of bacteria, where cells
620 become highly activated and M1-polarized through TLR signalling⁶⁵ and potent Nuclear Factor
621 (NF)- κ B activation,⁶⁶ which results in the production of inflammatory cytokines and soluble
622 factors contributing to polarization. Autophagy signaling may also be responsible for prolonging
623 phagocyte survival, which was the case for internalization of apoptotic cells and survival resulting
624 from interactions with mitogen-activated protein kinases (MAPK) pathways.⁶⁷ Phagocyte survival
625 associated with autophagy or TLR signaling is potentially initiated at the phagocytic synapse;
626 likely the M1 activation stemming from the acidic degradation components serves to synergize
627 with pro-survival signaling to enhance viability.⁶⁸ Thus, the polarization observed following
628 PEGDA NP internalization and resultant M1 polarization is expected to enhance pro-survival
629 signaling to directly influence cell fate.

630
631 To gain deeper insight on these NP degradation-induced macrophage longevity profiles,
632 potentially immunomodulatory NP degradation products must be investigated in future studies.
633 Immunostimulatory HS-PEG-SH-based degradable formulations are in contrast to
634 immunosuppressive properties of other particle chemistries such as PLGA, where lactic acid
635 degradation products are hypothesized to suppress M1 phenotypical changes,⁶⁰ but are in
636 agreement with M1-like polarization as a result of degradable PBAE particles.⁵⁸ Therefore, NP
637 chemistry and the specific nature of NP degradation products may play a critical role in
638 macrophage activation and the resultant pro-survival mechanisms. Our work draws attention to
639 this important influence of NP-induced phagocyte longevity enhancement and the link to various
640 physiochemical properties that requires future evaluations.

641

642

643

644 Conclusion

645 In this study, we report that degradation rate and resultant degradation products of PEG-based NPs
646 are critical parameters for tuning the survival of *ex vivo* primary macrophages. NPs with higher
647 degradation rates show dramatic effects in stimulating M1-like macrophage activation markers in
648 the absence of inflammatory cytokine secretions, corresponding to *in vitro* evaluations of mass-
649 based NP degradation. Lysosomal stimulation is dramatically enhanced in the presence of rapidly
650 degrading NPs compared to their slowly degrading counterparts. These phenomena are
651 hypothesized to be caused by the increased presence of degradation products in rapidly degrading
652 NP groups, which have been recently shown in other works to drive phenotypical changes in innate
653 immune cells. Further studies are needed to characterize PEG-based degradation products and
654 isolate their independent effects on primary macrophage longevity and activation state. In addition,
655 different degradable chemistries must be compared to better understand the impact of downstream
656 intracellular NP processing events on cell survival. This work opens the door to future
657 investigations of physiochemical properties of NP-based strategies aimed at tuning the survival
658 and function of macrophages and phagocytes for therapeutic applications and models.

659

660 Conflicts of interest

661 There are no conflicts of interest to declare.

662

663 Funding Information

664 Research reported in this publication was supported by the National Institutes of Health and the
665 State of Delaware under Award Number P20GM103446 and P20GM104316, as well as a Research
666 Starter Grant in Pharmaceuticals from the PhRMA Foundation, and a University of Delaware
667 Research Foundation Award. Z.S.S. was supported by a T32GM008550 training grant. The content
668 is solely the responsibility of the authors and does not necessarily represent the official views of
669 the National Institutes of Health.

670

671 Acknowledgements

672 TOC figure was created using biorender.com.

673 LC-MS was performed by Dr. P. Asare-Okai.

674 Cryo-SEM was performed with the assistance of D. Powell.

675 Thermo Scientific™ Apreo VS SEM microscope: Microscopy equipment was acquired with a
676 shared instrumentation grant (S10 OD025165) and access was supported by the NIH-NIGMS
677 (P20 GM103446), the NSF (IIA-1301765) and the State of Delaware.
678

679 **References**

- 680 1. R. Sridharan, A. R. Cameron, D. J. Kelly, C. J. Kearney and F. J. O'Brien, *Materials Today*,
681 2015, **18**, 313-325.
- 682 2. C. E. Witherel, K. Sao, B. K. Brisson, B. Han, S. W. Volk, R. J. Petrie, L. Han and K. L.
683 Spiller, *Biomaterials*, 2021, **269**, 120667.
- 684 3. K. L. Wofford, D. K. Cullen and K. L. Spiller, *Journal of Biomedical Materials Research*
685 *Part A*, 2019, **107**, 1213-1224.
- 686 4. B. M. Jarai, Z. Stillman, K. Bomb, A. M. Kloxin and C. A. Fromen, *ACS Biomater. Sci.*
687 *Eng.*, 2020, DOI: 10.1021/acsbiomaterials.0c01287.
- 688 5. E. C. Wayne, C. Long, M. J. Haney, E. V. Batrakova, T. M. Leisner, L. V. Parise and A. V.
689 Kabanov, *Advanced Science*, 2019, **6**, 1900582.
- 690 6. N. Shobaki, Y. Sato, Y. Suzuki, N. Okabe and H. Harashima, *Journal of Controlled Release*,
691 2020, **325**, 235-248.
- 692 7. B. M. Jarai, Z. Stillman, L. Attia, G. E. Decker, E. D. Bloch and C. A. Fromen, *ACS Applied*
693 *Materials & Interfaces*, 2020, **12**, 38989-39004.
- 694 8. S. Soares, J. Sousa, A. Pais and C. Vitorino, *Frontiers in Chemistry*, 2018, **6**.
- 695 9. B. M. Jarai, E. L. Kolewe, Z. S. Stillman, N. Raman and C. A. Fromen, in *Nanoparticles for*
696 *Biomedical Applications*, eds. E. J. Chung, L. Leon and C. Rinaldi, Elsevier, 2020, DOI:
697 <https://doi.org/10.1016/B978-0-12-816662-8.00018-7>, pp. 303-324.
- 698 10. J. W. Hickey, J. L. Santos, J.-M. Williford and H.-Q. Mao, *J Control Release*, 2015, **219**,
699 536-547.
- 700 11. J.-M. Williford, J. L. Santos, R. Shyam and H.-Q. Mao, *Biomater Sci*, 2015, **3**, 894-907.
- 701 12. D. Guo, G. Xie and J. Luo, *Journal of Physics D: Applied Physics*, 2013, **47**, 013001.
- 702 13. E. Fröhlich, *Int J Nanomedicine*, 2012, **7**, 5577-5591.
- 703 14. N. Kamaly, B. Yameen, J. Wu and O. C. Farokhzad, *Chem Rev*, 2016, **116**, 2602-2663.
- 704 15. A. E. Nel, L. Mädler, D. Velegol, T. Xia, E. M. V. Hoek, P. Somasundaran, F. Klaessig, V.
705 Castranova and M. Thompson, *Nature Materials*, 2009, **8**, 543-557.
- 706 16. J. A. Champion and S. Mitragotri, *Proc Natl Acad Sci U S A*, 2006, **103**, 4930.
- 707 17. R. A. Roberts, T. Shen, I. C. Allen, W. Hasan, J. M. DeSimone and J. P. Y. Ting, *PLOS*
708 *ONE*, 2013, **8**, e62115.
- 709 18. B. M. Jarai and C. A. Fromen, *bioRxiv*, 2021, DOI: 10.1101/2021.04.22.440822,
710 2021.2004.2022.440822.

- 711 19. P. Zhou, X.-L. Yang, X.-G. Wang, B. Hu, L. Zhang, W. Zhang, H.-R. Si, Y. Zhu, B. Li, C.-
712 L. Huang, H.-D. Chen, J. Chen, Y. Luo, H. Guo, R.-D. Jiang, M.-Q. Liu, Y. Chen, X.-R.
713 Shen, X. Wang, X.-S. Zheng, K. Zhao, Q.-J. Chen, F. Deng, L.-L. Liu, B. Yan, F.-X. Zhan,
714 Y.-Y. Wang, G.-F. Xiao and Z.-L. Shi, *Nature*, 2020, **579**, 270-273.
- 715 20. A. Parihar, T. D. Eubank and A. I. Doseff, *J Innate Immun*, 2010, **2**, 204-215.
- 716 21. L. M. Stuart and R. A. B. Ezekowitz, *Immunity*, 2005, **22**, 539-550.
- 717 22. W. K. E. Ip, A. Sokolovska, G. M. Charriere, L. Boyer, S. Dejardin, M. P. Cappillino, L. M.
718 Yantosca, K. Takahashi, K. J. Moore, A. Lacy-Hulbert and L. M. Stuart, *J Immunol*, 2010,
719 **184**, 7071-7081.
- 720 23. G. C. Baltazar, S. Guha, W. Lu, J. Lim, K. Boesze-Battaglia, A. M. Laties, P. Tyagi, U. B.
721 Kompella and C. H. Mitchell, *PLOS ONE*, 2012, **7**, e49635.
- 722 24. J. Zeng, A. Martin, X. Han, O. S. Shirihai and M. W. Grinstaff, *Industrial & Engineering*
723 *Chemistry Research*, 2019, **58**, 13910-13917.
- 724 25. C. A. Fromen, T. B. Rahhal, G. R. Robbins, M. P. Kai, T. W. Shen, J. C. Luft and J. M.
725 DeSimone, *Nanomedicine: Nanotechnology, Biology and Medicine*, 2016, **12**, 677-687.
- 726 26. C. He, Y. Hu, L. Yin, C. Tang and C. Yin, *Biomaterials*, 2010, **31**, 3657-3666.
- 727 27. R. Nicolete, D. F. d. Santos and L. H. Faccioli, *International Immunopharmacology*, 2011,
728 **11**, 1557-1563.
- 729 28. C. D. Walkey, J. B. Olsen, H. Guo, A. Emili and W. C. W. Chan, *Journal of the American*
730 *Chemical Society*, 2012, **134**, 2139-2147.
- 731 29. S. L. Demento, W. Cui, J. M. Criscione, E. Stern, J. Tulipan, S. M. Kaech and T. M. Fahmy,
732 *Biomaterials*, 2012, **33**, 4957-4964.
- 733 30. N. Chen, M. M. Johnson, M. A. Collier, M. D. Gallovic, E. M. Bachelder and K. M. Ainslie,
734 *J Control Release*, 2018, **273**, 147-159.
- 735 31. X. Xie, J. Wang, L. Zhang, S. Zeng, X. Su and Q. Chen, *Bioconjugate Chemistry*, 2021,
736 DOI: 10.1021/acs.bioconjchem.1c00171.
- 737 32. J. A. Hamilton, *Journal of Leukocyte Biology*, 2003, **73**, 702-712.
- 738 33. B. S. Zolnik, A. González-Fernández, N. Sadrieh and M. A. Dobrovolskaia, *Endocrinology*,
739 2010, **151**, 458-465.
- 740 34. S. Su and P. M. Kang, *Nanomaterials (Basel)*, 2020, **10**.
- 741 35. S. Rezvantalab, N. I. Drude, M. K. Moraveji, N. Güvener, E. K. Koons, Y. Shi, T. Lammers
742 and F. Kiessling, *Front Pharmacol*, 2018, **9**.

- 743 36. T. M. Fahmy, S. L. Demento, M. J. Caplan, I. Mellman and W. M. Saltzman, *Nanomedicine*,
744 2008, **3**, 343-355.
- 745 37. J. Da Silva, S. Jesus, N. Bernardi, M. Colaço and O. Borges, *Frontiers in Bioengineering and*
746 *Biotechnology*, 2019, **7**.
- 747 38. B. K. Lee, Y. Yun and K. Park, *Advanced Drug Delivery Reviews*, 2016, **107**, 176-191.
- 748 39. A. Kumari, S. K. Yadav and S. C. Yadav, *Colloids and Surfaces B: Biointerfaces*, 2010, **75**,
749 1-18.
- 750 40. E. Malikmammadov, T. E. Tanir, A. Kiziltay, V. Hasirci and N. Hasirci, *Journal of*
751 *Biomaterials Science, Polymer Edition*, 2018, **29**, 863-893.
- 752 41. Z. Stillman, B. M. Jarai, N. Raman, P. Patel and C. A. Fromen, *Polymer Chemistry*, 2020, **11**,
753 568-580.
- 754 42. A. Pelfrêne, M. R. Cave, J. Wragg and F. Douay, *Int J Environ Res Public Health*, 2017, **14**,
755 112.
- 756 43. X. Zhang, R. Goncalves and D. M. Mosser, *Curr Protoc Immunol*, 2008, **Chapter 14**, Unit-
757 14.11.
- 758 44. D. L. Kurdikar and N. A. Peppas, *Polymer*, 1994, **35**, 1004-1011.
- 759 45. H. Chikaura, Y. Nakashima, Y. Fujiwara, Y. Komohara, M. Takeya and Y. Nakanishi,
760 *Biosurface and Biotribology*, 2016, **2**, 18-25.
- 761 46. M. O. Oyewumi, A. Kumar and Z. Cui, *Expert Rev Vaccines*, 2010, **9**, 1095-1107.
- 762 47. E. Joseph and G. Singhvi, in *Nanomaterials for Drug Delivery and Therapy*, ed. A. M.
763 Grumezescu, William Andrew Publishing, 2019, DOI: [https://doi.org/10.1016/B978-0-12-](https://doi.org/10.1016/B978-0-12-816505-8.00007-2)
764 [816505-8.00007-2](https://doi.org/10.1016/B978-0-12-816505-8.00007-2), pp. 91-116.
- 765 48. O. Lunov, T. Syrovets, C. Loos, J. Beil, M. Delacher, K. Tron, G. U. Nienhaus, A.
766 Musyanovych, V. Mailänder, K. Landfester and T. Simmet, *ACS Nano*, 2011, **5**, 1657-1669.
- 767 49. M. A. Dobrovolskaia and S. E. McNeil, *Nature Nanotechnology*, 2007, **2**, 469-478.
- 768 50. J. R. Griffiths, *British Journal of Cancer*, 1991, **64**, 425-427.
- 769 51. Y. Ishida, S. Nayak, J. A. Mindell and M. Grabe, *J Gen Physiol*, 2013, **141**, 705-720.
- 770 52. H. B. Fleit and M. B. Furie, in *Pathobiology of Human Disease*, eds. L. M. McManus and R.
771 N. Mitchell, Academic Press, San Diego, 2014, DOI: [https://doi.org/10.1016/B978-0-12-](https://doi.org/10.1016/B978-0-12-386456-7.01807-4)
772 [386456-7.01807-4](https://doi.org/10.1016/B978-0-12-386456-7.01807-4), pp. 289-299.
- 773 53. A. Tang, Y. Wang, H. Ye, C. Zhou, C. Yang, X. Li, H. Peng, F. Zhang, Y. Hou and F. Teng,
774 *Nanotechnology*, 2013, **24**, 355602.

- 775 54. F. Hoelscher, P. B. Cardoso, G. Candiotto, C. Guindani, P. Feuser, P. H. H. Araújo and C.
776 Sayer, *Journal of Polymers and the Environment*, 2021, DOI: 10.1007/s10924-021-02139-w.
- 777 55. R. J. Clem, E. H. Y. Cheng, C. L. Karp, D. G. Kirsch, K. Ueno, A. Takahashi, M. B. Kastan,
778 D. E. Griffin, W. C. Earnshaw, M. A. Veluona and J. M. Hardwick, *Proc Natl Acad Sci U S*
779 *A*, 1998, DOI: 10.1073/pnas.95.2.554.
- 780 56. H. Lin, C. Chen and B. D. Chen, *Biochem J*, 2001, **353**, 299-306.
- 781 57. D. M. Sansom, *Immunology*, 2000, **101**, 169-177.
- 782 58. J. I. Andorko, K. L. Hess, K. G. Pineault and C. M. Jewell, *Acta Biomaterialia*, 2016, **32**, 24-
783 34.
- 784 59. D. A. Hume, D. M. Underhill, M. J. Sweet, A. O. Ozinsky, F. Y. Liew and A. Aderem, *BMC*
785 *Immunology*, 2001, **2**, 11.
- 786 60. R. P. Allen, A. Bolandparvaz, J. A. Ma, V. A. Manickam and J. S. Lewis, *ACS Biomater. Sci.*
787 *Eng.*, 2018, **4**, 900-918.
- 788 61. H. H. Gustafson, D. Holt-Casper, D. W. Grainger and H. Ghandehari, *Journal*, 2015, DOI:
789 10.1016/j.nantod.2015.06.006.
- 790 62. F. Sparber, J. M. Scheffler, N. Amberg, C. H. Tripp, V. Heib, M. Hermann, S. P. Zahner, B.
791 E. Clausen, B. Reizis, L. A. Huber, P. Stoitzner and N. Romani, *Blood*, 2014, DOI:
792 10.1182/blood-2013-08-518555.
- 793 63. S.-y. Zhu, R.-q. Yao, Y.-x. Li, P.-y. Zhao, C. Ren, X.-h. Du and Y.-m. Yao, *Cell Death &*
794 *Disease*, 2020, **11**, 817.
- 795 64. E. S. Trombetta, M. Ebersold, W. Garrett, M. Pypaert and I. Mellman, *Science*, 2003, **299**,
796 1400.
- 797 65. J. Baran, K. Guzik, W. Hryniewicz, M. Ernst, H. D. Flad and J. Pryjma, *Infection and*
798 *Immunity*, 1996, **64**, 4242-4248.
- 799 66. E. Lombardo, A. Alvarez-Barrientos, B. Maroto, L. Boscá and U. G. Knaus, *The Journal of*
800 *Immunology*, 2007, **178**, 3731.
- 801 67. S. M. Reddy, K. H. K. Hsiao, V. E. Abernethy, H. Fan, A. Longacre, W. Lieberthal, J.
802 Rauch, J. S. Koh and J. S. Levine, *The Journal of Immunology*, 2002, **169**, 702.
- 803 68. M.-Y. Wu and J.-H. Lu, *Cells*, 2019, **9**, 70.
804